Varying discharge controls on timescales of autogenic storage and release processes in fluvio-deltaic environments: Tank experiments

Erica J. Powell,[1] Wonsuck Kim,[1] and Tetsuji Muto[2]

Received 19 May 2011; revised 16 February 2012; accepted 28 February 2012; published 21 April 2012.

[1] Changes in external forcing have traditionally been the main areas of interest in understanding sedimentary records, while in most stratigraphic interpretation, autogenic behavior has been thought of as a "noise" generator. This study aims to investigate autogenic processes in a fluvio-deltaic system under a range of discharge conditions and to show that autogenic processes generate distinct signatures rather than random noise. A matrix of nine different experiments is presented here to systematically evaluate the effects of sediment and water discharge variations on the timescale of fluvial autogenic processes. Temporary sediment storage regularly occurs by backfilling of sediment in the fluvio-deltaic channels, followed by a period of strong channelization that releases the stored sediment. These storage and release processes cycle along with changes in the fluvial slope and planform pattern of the flow. Here we propose that the autogenic behavior of deltaic progradation has a distinct timescale that is controlled by sediment and water discharges. An increase in sediment discharge primarily reduces the autogenic timescale as higher sediment supply fills the channels faster. In contrast, the high sediment discharge causes a morphologic feedback by increasing the magnitude of fluvial slope change between the storage and release events and increasing the size of the temporary sediment storage (termed "the fluvial envelope"). This works against the sediment discharge control as the autogenic timescale is increased. Increasing the water discharge increases the autogenic timescale by improving the fluvial organization toward a strongly channelized system. Changes in autogenic timescale due to variations in the sediment and water discharges are nonlinear for different sediment to water discharge ratios. As the ratio decreases, the fluvial system is better organized and the timescale is more linearly related to the change in sediment discharge. As the ratio increases, deltas develop poorly organized fluvial systems and the associated timescales converge even with different sediment discharges. The results presented here provide enhanced interpretation of sedimentary records by better decoupling of autogenic signatures from allogenic products developed across a wide range of discharge conditions.

Citation: Powell, E. J., W. Kim, and T. Muto (2012), Varying discharge controls on timescales of autogenic storage and release processes in fluvio-deltaic environments: Tank experiments, *J. Geophys. Res.*, *117*, F02011, doi:10.1029/2011JF002097.

1. Introduction

[2] Sedimentary processes and their resulting stratigraphic architecture provide crucial clues to paleo-depositional environments. The rock record consists of sedimentary patterns that were developed due to changes in allogenic conditions as well as patterns that were developed autogenically (i.e., delta lobe/channel avulsion, sediment storage and release). *Muto et al.* [2007] defined the term 'autogenic' as intrinsic responses to steady external forcing and 'allogenic' as responses to non-steady external forcing. Traditionally, shoreline migration and stratigraphic sequences were attributed to unsteady changes in external dynamic factors (i.e., global sea-level changes, tectonic subsidence/uplift, and sediment supply changes) [*Galloway*, 1989a, 1989b; *Helland-Hansen and Gjelberg*, 1994; *Helland-Hansen and Martinsen*, 1996; *Posamentier and Vail*, 1988; *Posamentier et al.*, 1988; *Vail et al.*, 1977; *Van Wagoner et al.*, 1988; *Watts*, 1982]. Decoupling these allogenic signatures (externally driven) from autogenic variations (internally generated), is key to correctly decipher paleo-environmental variations in the sedimentary record. Autogenic products in the sedimentary record have not been thoroughly quantified and have generally been thought of as minor "noise" [*Kim*

[1]Department of Geological Sciences and Institute for Geophysics, Jackson School of Geosciences, University of Texas at Austin, Austin, Texas, USA.
[2]Graduate School of Fisheries Science and Environmental Studies, Nagasaki University, Nagasaki, Japan.

Copyright 2012 by the American Geophysical Union.
0148-0227/12/2011JF002097

and Jerolmack, 2008]. However, recent studies shown that internally generated responses can be cyclic in nature, and they play an important role in the sedimentary record in concert with variations of external forcing [*Ashworth et al.*, 2004; *Bryant et al.*, 1995; *Cazanacli et al.*, 2002; *Heller et al.*, 2001; *Hickson et al.*, 2005; *Jerolmack and Mohrig*, 2005; *Kim and Jerolmack*, 2008; *Kim and Muto*, 2007; *Kim and Paola*, 2007; *Kim et al.*, 2006a; *Kleinhans*, 2005; *Kleinhans et al.*, 2010b; *Mohrig et al.*, 2000; *Muto and Steel*, 2001, 2004; *Paola*, 2000; *Paola et al.*, 2001, 2009; *Sheets et al.*, 2002; *Van Dijk et al.*, 2009]. Non-steady external forcing (variation in the rate of base-level rise or variation in sediment supply conditions) is an important control on sedimentary processes and stratigraphic architectures; however, autogenic responses during both steady and non-steady external conditions should also be considered. In the present study, internal responses during steady external forcing are analyzed. Quantitative understanding of autogenic processes and their stratigraphic deposits will offer a more fundamental understanding of the stratigraphic record, as this facilitates the separation of stratigraphic data into allogenic and autogenic products.

[3] Experimental stratigraphy [*Paola et al.*, 2001] and flume/tank experiments provide a useful tool for understanding large-scale stratigraphic and morphodynamic responses and also for beginning to understand how to separate allogenic and autogenic signatures in the rock record [*Gerber et al.*, 2008; *Heller et al.*, 2001; *Hickson et al.*, 2005; *Kim et al.*, 2006b, 2010; *Kim and Paola*, 2007; *Kostic et al.*, 2002; *Martin et al.*, 2009a; *Muto*, 2001; *Muto and Steel*, 2001, 2004; *Muto and Swenson*, 2006; *Reitz et al.*, 2010; *Van Dijk et al.*, 2009; *Whipple et al.*, 1998]. Recent studies using tank experiments have demonstrated distinct shoreline position fluctuations due to autogenic fluvial sediment storage and release [*Kim and Jerolmack*, 2008; *Reitz et al.*, 2010; *Van Dijk et al.*, 2009]. *Ashmore* [1991] has suggested a similar process of internally generated pulses due to aggradation and degradation in braided, gravel bed streams. In these previous experiments, under constant sediment supply and upstream water discharge settings, the topset of deltas (and/or fans) show alternating periods of more sheet-like flow and strongly channelized flow. Here, sheet-like flow is referred to as overland flow by *Hogg* [1982], which is a relatively high-frequency and low-magnitude moving body of water that has the form of a thin and continuous film at the laminar regime. This flow pattern alternation causes fluctuations in the shoreline migration rate over time with an overall progradational trend in the experimental deltas. These flow conditions can be found in alluvial fan or fan delta environments such as the Kosi River fan in Northern India [*Reitz et al.*, 2010]. These fluctuations occur at regular intervals and they are caused by the cyclic nature of fluvial-mass storage (sheet flow) and release (channelization). During times of sheet flow, the flow widens and becomes laterally unconfined, which enhances deposition on the topset surface of the delta and causes a convex-up fluvial profile. Because most of the sediments are being stored on the topset surface, sediments are not being fed into the basin, which causes a slowly prograding or stationary shoreline. This alluvial aggradation steepens the overall slope of the delta topset until a critical threshold slope value is reached. At this time, the slope is steep enough for incision to inevitably occur so that the topset slope is reduced [*Parker et al.*, 1998]. The slope is maximized where a convex-up fluvial profile upstream meets a concave-up fluvial profile, and channel initiation occurs at this inflection point, migrating upstream as a knickpoint [*Kim and Jerolmack*, 2008; *Van Dijk et al.*, 2009]. A period of strong channelization begins to release sediments into the basin due to an increase in transport capability. An increased amount of sediment is transported during enhanced channelization due to the nonlinearity of sediment transport relations [*Parker et al.*, 1998]. This produces a great increase in the rate of the shoreline progradation. Eventually, cutting of the deltaic topset due to channelization, which is more focused upstream, reduces the overall topset slope of the delta to a point where backfilling of the channel begins to occur. Sheet flow deposition resumes again once the channel is filled with supplied sediment. Alternations between sheet flow and channelized flow produces cyclic fluctuations in the shoreline progradation rate and the topset slope through time. The alluvial slope of a delta is an important control in this process, and has been shown to be inversely related to water discharge, secondarily related to sediment supply [*Whipple et al.*, 1998], and linearly correlated to the sediment supply to water discharge ratio [*Parker et al.*, 1998].

[4] While these studies from *Kim and Jerolmack* [2008] and *Van Dijk et al.* [2009] have shown quantitative data illustrating this cyclic process of sediment storage and release, there are some missing experiments to fully understand the autogenic processes that the present study aims to complete. *Kim and Jerolmack* [2008] used two different experiments that kept sediment supply (Q_s) to water discharge (Q_w) ratios constant ($Q_s/Q_w \approx 0.01$) which caused similar overall deltaic surface slopes; however, different absolute values of sediment and water discharges were used. *Van Dijk et al.* [2009] ran three different experiments with constant Q_s, but varied the Q_w to explore how changes in water discharge affected this process. In the present study, a matrix of nine different experiments allowed for robust analysis of solely the effects of changes in Q_s, Q_w, and Q_s/Q_w on the autogenic storage and release processes. Quantitative measurements of the storage and release processes were obtained from the changes in shoreline migration rate. An analytical model was also used to extract the autogenic variations from the overall shoreline progradational trend. The effects of the Q_s/Q_w ratio, Q_s, and Q_w on the autogenic timescale (T_A) were explored and correlated to morphological changes in the fluvio-deltaic system. We also discussed implications of the understanding in the autogenic timescale for terrace development as well as significance for source to sink sediment deposition from the fluvio-deltaic to deep-water turbidite systems.

2. Experiment

2.1. Experimental Setup

[5] For this study, a matrix of nine different experiments was used to test the effects of Q_s, Q_w, and Q_s/Q_w on autogenic storage and release timescales (Figure 1). All of the experiments were conducted in a basin with dimensions of 1 m wide and 1 m long at Nagasaki University, Japan (Figure 2). Each experiment used a mixture of sediment and

RunName Q_w/Q_s / Run Time		Water Discharge (Q_w) → 16.2 cm³/s	32.5 cm³/s	65.0 cm³/s
Sediment Discharge (Q_s) ↓	0.5 cm³/s	LwLs *0.061* 7 hours	MwLs *0.03* 7 hours	HwLs *0.015* 6.18 hours
	1.0 cm³/s	LwMs *0.123* 5 hours	MwMs *0.061* 4.16 hours	HwMs *0.03* 4.3 hours
	2.0 cm³/s	LwHs *0.246* 3 hours	MwHs *0.123* 3 hours	HwHs *0.061* 2.5 hours

Figure 1. Experimental design matrix depicting the experimental design and Q_s/Q_w ratios. Three values of Q_w and three values of Q_s were used to yield nine experiments with different parameters. The experiment identifiers are shown in the upper portion of each box. The overall Q_s/Q_w ratios are shown in the center, and the total experimental run time is shown at the bottom.

water that was delivered into the basin, building a delta over a flat, non-erodible basement into a standing body of water. The sediment mixture contained two different grain sizes and used 50% fine sand (D = 0.1 mm and density = 2.27 g/cm^3) and 50% coarse sand (D = 1 mm and density = 2.92 g/cm^3) by volume. The sediment was pre-mixed with water and fed into the basin as a point source, located in the corner of the experimental basin. A 1.2 cm thick gravel layer was placed over the basement floor before each experiment to ensure a flat surface. Base level for these experiments was kept constant at 1.8 cm measured from the top of the gravel layer, and no subsidence was applied. Using constant external factors throughout each experimental run allowed for analysis of only the autogenic variation. The only changing elements between experiments were sediment supply and water discharge. The total run time for the different experiments varied because different sediment discharge values filled up the basin at different rates, but each delta was built to about 80–90 cm away from the sediment and water point source. This allowed development of 4–8 autogenic cycles. The experimental parameters are shown in Table 1. The sediment discharge values ranged from 0.5 cm^3/s (low Q_s runs) to 2 cm^3/s (high Q_s runs). For the water discharge, 65 cm^3/s was used for the highest discharge runs and 16.25 cm^3/s was used for the lowest discharge runs. This yielded Q_s/Q_w values that range from 0.015 at the lowest to 0.246 at the highest. The individual experiments will be referred to by acronyms that pertain to the sediment and water input parameters for the particular experiment. For instance, the experiment at the bottom right hand corner of the design matrix (Figure 1) has a high value for water discharge (65 cm^3/s) and a high value for sediment discharge (2 cm^3/s). This experiment will be referred to as HwHs because of the high water value and high sediment value. A low water discharge run (16.25 cm^3/s) with a medium sediment discharge (1 cm^3/s) will be referred to as LwMs, a medium water discharge run (32.5 cm^3/s) with a low sediment discharge (0.5 cm^3/s) will consequently be referred to as MwLs, and so on.

2.2. Methods and Data Set

[6] In order to capture the deltaic evolution, high-resolution time-lapse overhead photos were taken every 20 s for each experiment (Figure 3a). The water was dyed a blue color in order to increase visibility. The blueness in the photos was first converted to gray scale, and then to black and white images using a certain threshold value. This threshold value is a water depth proxy which allowed for the experimental deltaic surface to be starkly contrasted with the standing water (ocean), outlining the shoreline for each image (Figures 3a and 3b). The shoreline was mapped automatically using each of the black and white images (Figures 3c and 3d). A laterally averaged shoreline position was extracted from the overall mapped shoreline by using the average length of each shoreline point away from the point source location for each image. This produced an average shoreline position through time for each experiment.

[7] Laser lines were projected horizontally onto the deltaic surface at different heights (1 cm and 2.5 cm from base level). These laser lines acted as topographic lines of equal elevation that were used to measure the slope of the topset surface of the experimental delta. Three known elevations (base level and two topographic lines) allowed for detailed slope measurements over the topset of the delta. For every 15 images (i.e., every 5 min of experimental run time), the slopes were measured along three different transects on the top of the deltaic surface when the delta had built to a sufficient size. Three different slope measurements were collected along each transect. This ensured more accurate values for the topset slope (S_t) both through time and overall for each experiment. The slope of the foreset (S_f) was also

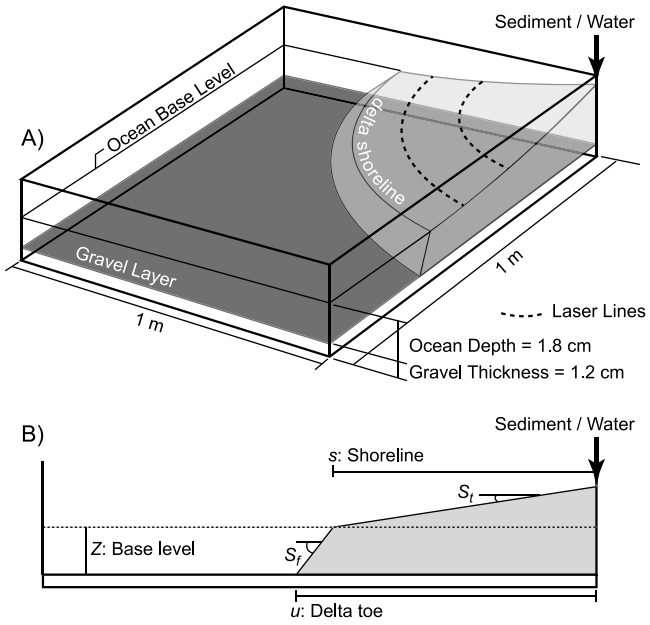

Figure 2. (a) Schematic diagram of the experimental setup. (b) Definition sketch for model parameters.

Table 1. Experimental Parameters

Experiment Run Name	Q_s/Q_w	Q_s (cm^3/s)	Q_w (cm^3/s)	Average Slope (S_t)	Run Time (h)	Frequency (cycle/h)	Timescale T_A (h)	Frequency (normalized)	Timescale T_A/T_{DC}
HwLs	0.015	0.5	65.0	0.043	6.18	1.20	0.833	0.053	18.779
HwMs	0.030	1.0	65.0	0.058	4.30	1.69	0.592	0.049	20.137
HwHs	0.060	2.0	65.0	0.077	2.50	2.02	0.495	0.039	25.273
MwLs	0.030	0.5	32.5	0.058	7.00	1.40	0.714	0.082	12.154
MwMs	0.060	1.0	32.5	0.077	1.16	1.65	0.606	0.065	15.470
MwHs	0.123	2.0	32.5	0.103	3.00	2.00	0.500	0.052	19.210
LwLs	0.060	0.5	16.2	0.077	7.00	1.71	0.585	0.133	7.464
LwMs	0.123	1.0	16.2	0.103	5.00	2.00	0.500	0.104	9.605
LwHs	0.246	2.0	16.2	0.136	3.00	2.40	0.417	0.083	12.088

measured, but showed much less variability than the topset slope. This slope was measured using the known water surface elevation and the known basement elevation along the three different transects; however, due to the more consistent nature of the foreset, the slopes were measured every 50 images.

2.3. Experimental Results

[8] Each of the nine experiments shows a progradational shoreline migration trend (Figure 4). Because base level remained stationary, the fluvial topset also remained aggradational [*Muto et al.*, 2007]. Figure 4 indicates that autogenic events are superimposed over the long-term progradational trend. A small-scale increase in the rate of shoreline progradation compared to the general migration trend indicates a time of autogenic release due to strong channelization. However, when this curve shows a slower or stagnate rate of progradation, a period of storage is dominant [*Kim and Jerolmack*, 2008]. Due to different overall values of sediment supply and water discharge, the rate of progradation differs among the nine experiments. The plots from Figure 4 show that the overall rate of progradation is similar among experiments with the same sediment supply even though different amounts of water discharge alters the steepness of the topset slope and lead to slightly different overall shoreline migration trends. The importance of sediment supply versus water discharge in the autogenic storage and release timescales will be discussed in more detail.

[9] Changes in map-view patterns of the shoreline geometry can be seen in the experimental time-lapse images. The

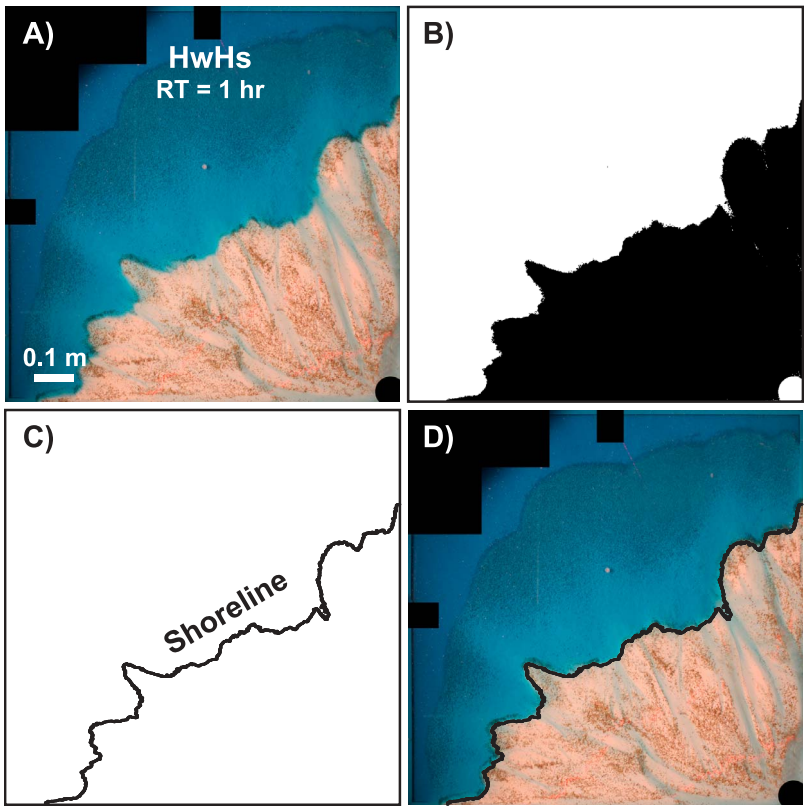

Figure 3. (a) Overhead image taken from experiment HwHs at run time (RT) = 1 h, prior to any manipulation, (b) image as a result of automatic color manipulation. Deltaic surface is black and ocean is white showing a clearly defined shoreline, (c) resulting mapped shoreline, and (d) original image overlain by the automatically extracted shoreline.

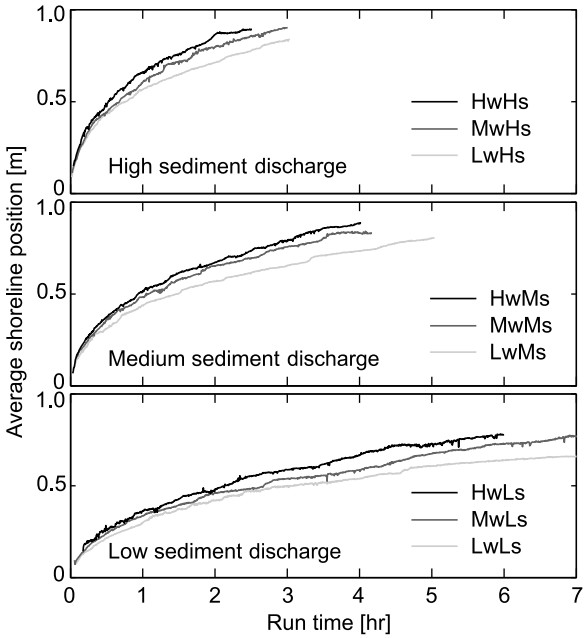

Figure 4. All nine experiments grouped by runs that have constant sediment discharge. From top to bottom, high sediment discharge, medium sediment discharge, and low sediment discharge.

experimental deltas showed either highly rough-shoreline (i.e., highly deviated from a semi-circular shoreline with an averaged downstream location) or quite smooth-shoreline geometry. Most likely, the roughness is linked to the Q_s/Q_w ratio. More stable channels were seen in concert with the low Q_s/Q_w ratios, which allowed for strong delta lobe development and local shoreline perturbations in planform. However, in the Q_s/Q_w ratio runs, the shoreline roughness decreased as the dominant channelization was only sustained over a short time period, and the deltaic surface was dominated by distributary channels and/or sheet flows. Figures 5a and 5b show an example of different shoreline geometries observed in HwLs and LwLs, respectively, ranging from quite rough (with delta lobe development at the center of the basin), to more smooth and symmetrical (with sheet-like flow covering a wide range of the surface).

[10] The slope range for each experiment was calculated using the 10th and 90th percentiles of averaged downstream slopes measured along the three transects using the known three topographic elevations (see the slope measurement in the methods and data set section). This range is indicative of how much space exists between the highest level of aggradation (highest slope) and the lowest level of sediment release by channelization (lowest slope). The slope range can also be described as a buffer, as defined by *Holbrook et al.* [2006] in which the term buffer was proposed to describe conceptual surfaces: (1) the potential maximum aggradational surface and (2) the maximum level of incision in a longitudinal river profile. While the application of the term "buffer" in this study does not meet the definition of *Holbrook et al.* [2006] exactly, a similar conceptualization can be utilized with the two dynamic fluvial profiles that occur during sediment storage and release [*Kim et al.*, 2006a]. The space between these two buffers encases the available fluvial envelope, and here it is shown that the magnitude of this space changes with changing Q_s/Q_w ratios (Figure 6). A positive relationship exists between these two factors, indicating that the space created during a storage and release cycle, increases with increasing Q_s/Q_w ratio. Theoretically, if sediment is negligible in the system, no storage and release processes would occur. In contrast, the rate of increase in the buffer size diminishes with an increase in the Q_s/Q_w ratio as the topographic slope gets close to the angle of repose (Figure 6).

3. Geometric Shoreline Model

3.1. Analytical Model Derivation

[11] A simple geometric model was developed in order to mathematically model the shoreline position through time

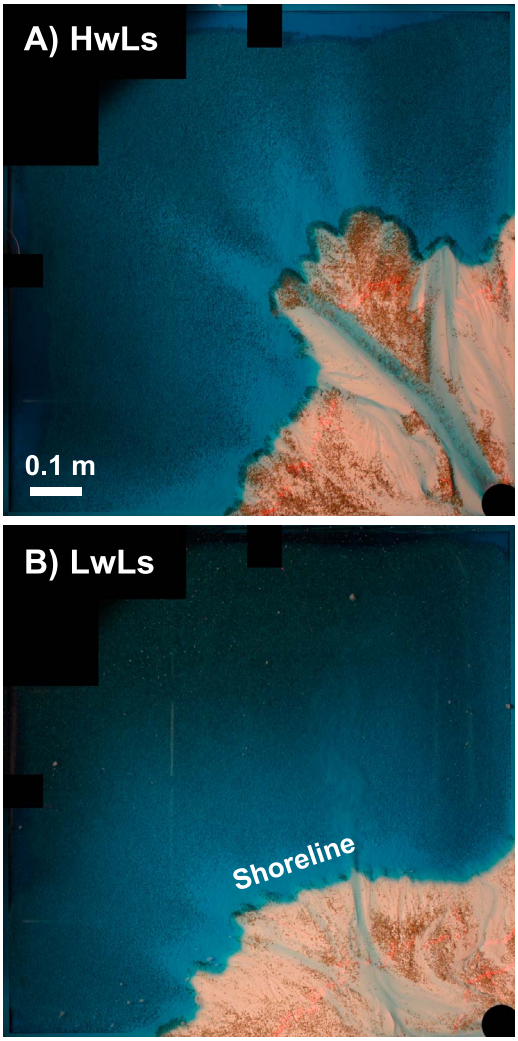

Figure 5. (a) Photo taken from HwLs (RT = 2.3 h) during a release event, with a low Q_s/Q_w ratio, showing a rough shoreline with delta lobe protrusion and a deep, straight channel. (b) Photo taken from LwLs (RT = 3 h) during a release event, with a high Q_s/Q_w, showing a smoother shoreline, with no significant lobe formation and a highly disorganized channel system.

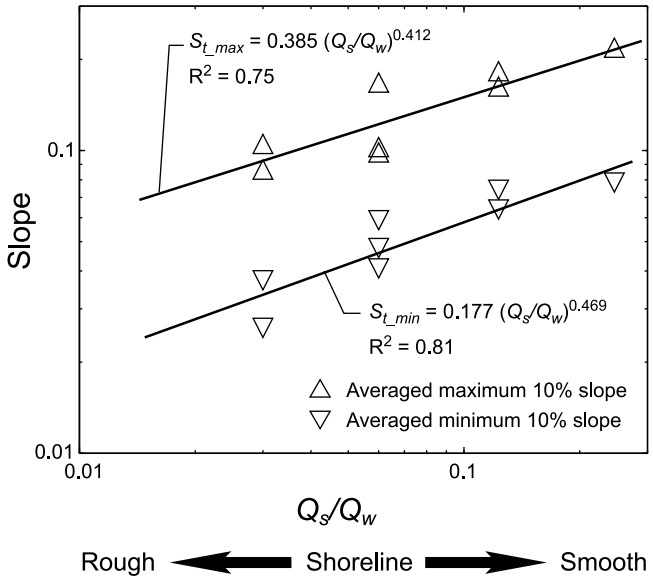

Figure 6. Average minimum slope S_{t_min} and maximum slope S_{t_max} associated with each Q_s/Q_w ratio. Shoreline roughness is defined as the qualitative shoreline geometry observed.

to accompany the experimental data. This model aims to capture the general progradational trend as a moving boundary [*Swenson et al.*, 2000] and not the autogenic variation of the shoreline similar to the model presented by *Kim and Muto* [2007]. The definition sketch for the model parameters can be seen in Figure 2b. The delta deposit can be characterized into two different geometries: a cylinder and a cone. The cylinder shape approximates the bottom (submerged) deposit, while the cone shape approximates the top (subaerial) deposit assuming a linear surface slope. The geometrical assumption for a three-dimensional delta takes a similar form that has been used by *Muto and Okada* [1991] and *Kleinhans et al.* [2010a], and geometric models similar to that are presented here but in two dimensions have been applied to model deltaic evolution in scaled experiments and field studies [*Kim et al.*, 2006b; *Heller et al.*, 1993; *Petter and Muto*, 2008]. A balance between supplied sediment over a given time and deposited sediment, for which the total volume is a sum of (1) the volume of the top of the delta by using 1/4 the volume of a cone and (2) the volume of the bottom of the delta by using 1/4 the volume of a cylinder can be represented with the following form:

$$Q_s t = \frac{1}{4}\left[\frac{1}{3}\pi s^2 H + \pi Z\left(\frac{u-s}{2}\right)^2\right], \tag{1}$$

where s denotes the shoreline position, u denotes the delta toe position, Z denotes the base-level height (1.8 cm from the gravel layer), H denotes the height from base level to the highest upstream point, Q_s denotes the sediment discharge at the point source, and t denotes time. However, some parameters in this governing equation are unknowns (H and u). The slope components from the definition sketch can be used to substitute unknown variables for known, or measured parameters, to calculate the downstream shoreline position. The slope components here are

$$S_t = \frac{H}{s} \tag{2a}$$

$$S_f = \frac{Z}{u-s}, \tag{2b}$$

where S_t denotes the average linear topset slope, and S_f denotes the average foreset slope. Substituting relationships in (2a) and (2b) into the governing equation (1) yields

$$s^3 + 3\frac{Z}{S_t}s^2 + 3\frac{Z^2}{S_t S_f}s + \frac{3}{4}\left(\frac{Z^3}{S_t S_f}\right) = 12\frac{Q_s t}{S_t \pi}. \tag{3}$$

Solving for s will yield an equation for the position of the shoreline through time with known input and measured parameters. The cubic formula is used to find an equation for s in terms of these variables. The cubic formula involves defining coefficients for the third order polynomial above to solve for the wanted variable s

$$s = \sqrt[3]{\frac{\beta t - \alpha}{2} + \sqrt{\frac{(\alpha+\beta t)^2}{4} + \frac{p^3}{27}}} + \sqrt[3]{\frac{\beta t - \alpha}{2} - \sqrt{\frac{(\alpha+\beta t)^2}{4} + \frac{p^3}{27}}} - \frac{Z}{S_t}, \tag{4}$$

where

$$p = 3\left(\frac{Z}{S_t}\right)^2\left(\frac{S_t}{S_f} - 1\right), \tag{5a}$$

$$\alpha = \left(\frac{Z}{S_t}\right)^3\left[\frac{3}{4}\left(\frac{S_t}{S_f}\right)^2 - 3\frac{S_t}{S_f} + 2\right], \tag{5b}$$

$$\beta = -12\frac{Q_s}{S_t \pi}. \tag{5c}$$

Here it is assumed that Q_s, Z, S_t, and S_f are constant with time and thus p, α, and β are constant. The above formulation is algebraically complex; however, it is important to understand that the shoreline position (s) is modeled as a function of the cube root of time ($t^{1/3}$) in a radially growing delta.

3.2. Modeling Results

[12] The experimental parameters (Table 1) were applied to the analytical model derived above to capture the overall progradational trend of the experimental shoreline. As shown in the derivation, the shoreline position through time is a function of Q_s, Z, S_f, and S_t. Figure 7a shows an example of the analytical model compared with the actual shoreline position measured from the experiments (see auxiliary material for all other runs).[1] The model shows a monotonically prograding trend while the experimental model shows progradation along with autogenic fluctuations in the shoreline through time. This is significant because the model

[1]Auxiliary materials are available in the HTML. doi:10.1029/2011jf002097.

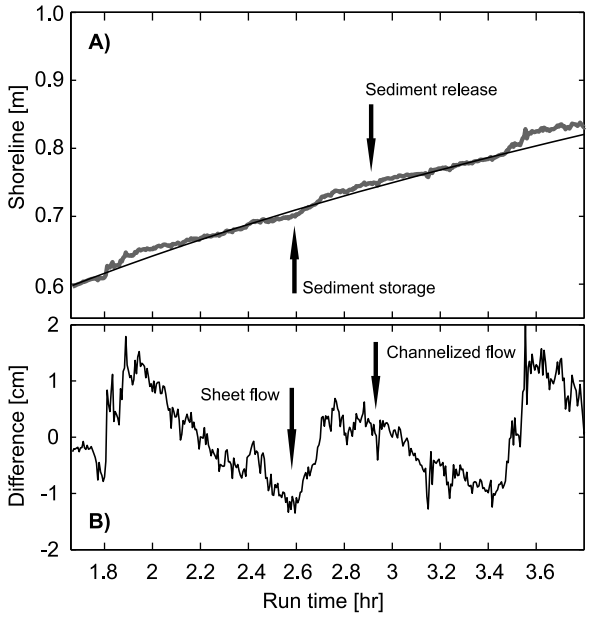

Figure 7. (a) From MwMs, (RT = 1.6–3.8 h), the experimental average shoreline position in the thick gray line and the analytically modeled shoreline position in the thin black line. (b) The difference between the analytically modeled shoreline and the experimental average shoreline with time. Fluctuations represent storage and release events. Peaks represent release events (when the average shoreline is greater than the analytically modeled shoreline) and troughs represent storage (when the average shoreline is less than the analytically modeled shoreline).

does not depict autogenic variability, but instead, it is a simplified geometric model that shows large-scale trends. Deviations from the overall trend are caused by autogenic storage and release events. In order to extract the autogenic fluctuations through time, the model results were used to de-trend the long-term shoreline migration component by differencing the two curves (Figure 7b). In this way, the fluctuations represented by troughs and peaks, respectively, shown in Figure 7b are due to solely autogenic storage and release events.

[13] This model captures the shoreline migration using the cube root of time relationship, instead of the square root of time that is often used in modeling two-dimensional deltaic evolution [*Reitz et al.*, 2010; *Lorenzo-Trueba et al.*, 2009; *Kim et al.*, 2006a; *Swenson et al.*, 2000]. Both relationships indicate that with external forcing held constant, deltas will initially prograde quickly, but the progradation rate nonlinearly decreases through time. Due to the three-dimensional nature of these experiments, it is important to capture the cube root function because this causes the shoreline migration rate to decrease faster than it would with a model using the square root of time.

3.3. Normalization

[14] The shoreline position and experimental run time data were both normalized in order to create dimensionless numbers that could be analyzed free from constraints of scale for individual experiments, using characteristic scales for length (L) and time (T_{DC}), respectively,

$$L = \frac{h}{S_t} \tag{6a}$$

$$T_{DC} = \frac{L^2 h}{Q_s}, \tag{6b}$$

where L is the characteristic backwater length, and h is the channel depth (assuming spatially uniform channels that are always bankfull). The flow depth ranges between ~1 mm and ~1 cm depending on the flow structure but the average channel depth during release events was approximately 1 cm. We applied this approximation for h uniformly to all runs, but the topset slopes (S_t) were taken from the averaged values for individual experiment, which are quite variable for the experimental conditions (Table 1). This is the same approach as presented by *Postma et al.* [2008], in which the equilibrium timescale is described by a characteristic volume representing the system and the characteristic transport rate (Q_s).

4. Autogenic Timescale

[15] As mentioned above, the de-trended shoreline time series data were used to quantitatively measure the autogenic fluctuations. Figure 7b shows the time series curve that represents deviations of the shoreline location from the overall trend derived from the analytical model, indicating that either dominant release or storage was occurring. Statistical methods and time series analysis were used in order to detect the number of peaks (release events) from the curve in concert with spectral plots showing different orders of frequencies in the data (Figure 8a and 8b, respectively). The first method used a certain window length to re-sample the time series data and extract the most significant trends. The main cycle frequency reflecting storage and release processes can then be manually picked for each experiment by using the number of release events that occur per hour of experimental run time (Figure 8a). Second, the spectral plot method shows different orders of cycle frequencies derived from a Fourier transformation (Figure 8b). This method automatically detected multiple hierarchy-order frequencies from the curve that results from autogenic processes. The most significant (or first-order frequency signal) is shown as the largest peak, and this was used to define the characteristic autogenic timescale associated with each experimental run. These two methods were used in concert with each other to ensure accurate autogenic timescale (T_A) measurements, which gives an approximate time period between release events. The timescale data was normalized by the characteristic timescale (i.e., T_A/T_{DC}) for each experiment to take a dimensionless form.

[16] Table 1 shows the autogenic frequencies/timescales associated with both real and normalized data for each experiment. For consistency, the autogenic timescale in this study was calculated for only the same duration of the experimental run in the normalized timescale. While the shorelines advanced with different rates for individual experiments, to gain the correct trend of internal timescale

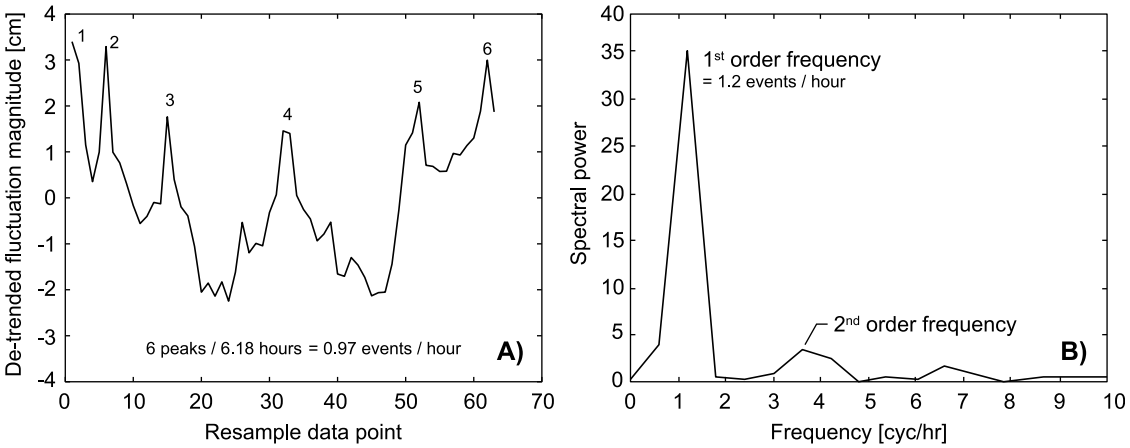

Figure 8. (a) Example of the re-sampling technique from HwLs showing six peaks, or release events and (b) example of the spectral plot for HwLs. The most significant frequency is the result of the autogenic storage and release cycles.

variation between experiments, it was important to normalize the times and to factor out the different overall rates of delta growth. In this way, we could use the consistent dimensionless time duration across the experiments.

[17] Experimental results show that as sediment discharge increases (Q_s/Q_w increases), the autogenic timescale also decreases (Table 1). This is evident for each of the three groups of experiments that have a constant water discharge and increasing sediment supply (Figure 9a). The groups of experiments with constant sediment supply, but varying water discharge values show that as water discharge decreases (Q_s/Q_w increases), the timescale for autogenic storage and release events also slightly decreases (Figure 9b). In general, the autogenic timescale decreases as Q_s/Q_w increases; however it is also observed that experiments with the same Q_s/Q_w ratio do not always show similar autogenic timescales (Figure 10a). This indicates that there are other factors affecting the autogenic timescale. Autogenic storage and release must depend on both (1) the

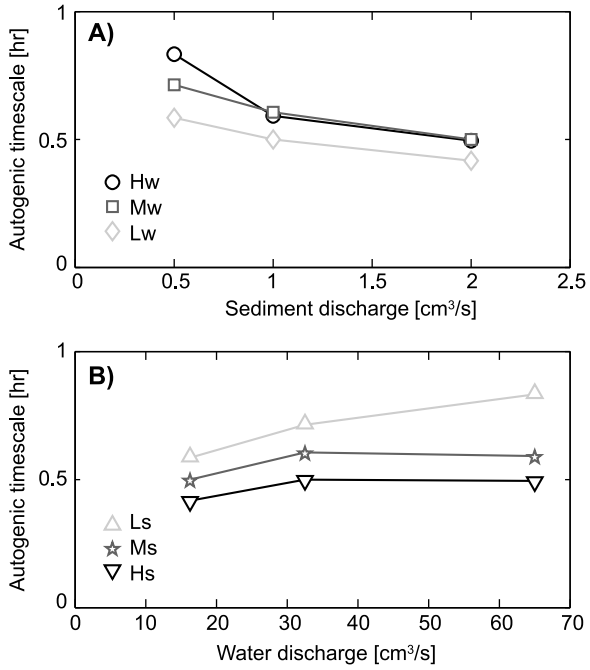

Figure 9. (a) Plot showing sediment discharge (cm^3/s) versus the autogenic timescale (h) grouped by experiments with constant water discharge. The autogenic timescale denotes that a characteristic duration between the fluvial sediment storage and release events. As sediment discharge increases (Q_s/Q_w increases), the timescale decreases. (b) Plot showing water discharge (cm^3/s) versus the autogenic timescale (h) grouped by experiments with constant sediment discharge. As water discharge increases, the timescale increases as a general trend.

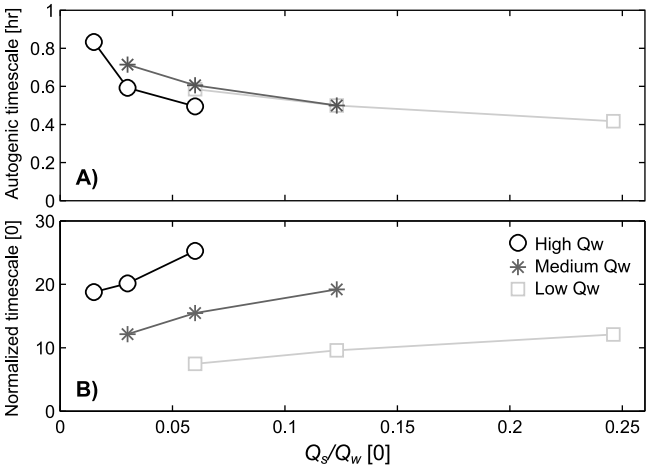

Figure 10. Plots showing the relationship between increasing sediment discharge (increasing Q_s/Q_w) and the autogenic timescale. (a) As the sediment supply increases, and Q_s/Q_w increases, the autogenic timescale decreases due to increasing sediment supply. (b) As sediment supply increases, and Q_s/Q_w increases, the normalized autogenic timescale increases indicating the increase in the size of the fluvial envelope during release events. The non-dimensional timescale was taken by dividing time by the equilibrium timescale calculated for individual experiment.

absolute values of Q_s and Q_w, and (2) their ratio. The trends of the normalized data for the autogenic timescale (Figure 10b) are slightly different than the non-normalized data, and this will be discussed in more detail.

5. Interpretation and Discussion

5.1. Role of Sediment Discharge on Autogenic Timescales

[18] A change in sediment discharge is an important control in fluvio-deltaic environments. It has been shown that an increase in sediment supply can (1) be a powerful driver for deltaic progradation even during times of base-level rise or highstand conditions [*Carvajal and Steel*, 2006], (2) increase channel mobility and confluence formation [*Ashmore*, 1991], and (3) be a factor in channel avulsion due to an increase in local deposition [*Martin et al.*, 2009b; *Mohrig et al.*, 2000]. Here, changes in sediment supply affect the frequency of autogenic storage and release events, i.e., the small pulses of change in the shoreline migration rate on an overall progradational shoreline trajectory. The frequency of the fluvial autogenic processes is closely related to the avulsion and/or delta lobe switching frequency, but here the analysis uses the laterally averaged shoreline of which three-dimensional effects are eliminated. The fluvial autogenic processes in this study encompass the fluvial activities such as lateral channel migration, avulsion, and lobe switching as a whole (see more description about the fluvial sediment storage and release processes in the works by *Kim et al.* [2006a] and *Kim and Jerolmack* [2008]).

[19] As sediment supply increases so too does the recurrence of autogenic release events. More sediment is available to fill the space created during release events and to increase the deltaic topset slope to a maximum critical value (i.e., the fluvial envelope). Therefore, the increased sediment supply shortens the time over which the fluvial envelope is filled and decreases the autogenic timescale (Figure 9a). This is consistent with the sediment discharge control on the avulsion period estimated by *Reitz et al.* [2010]. They estimated the avulsion timescale is inversely proportional to the sediment discharge and is proportional to the channel volume (the channel cross-sectional area times the fluvial length). However, as mentioned above, there is a secondary effect on modifying the fluvial envelope size due to change in sediment discharge. The envelope size (the space between the maximum and minimum topset slopes) is not equal for each Q_s/Q_w ratio, but instead, it increases as the Q_s/Q_w ratio increases (Figure 6). Using the difference between the average minimum ($S_{t_\min} = 0.177\ (Q_s/Q_w)^{0.469}$) and maximum ($S_{t_\max} = 0.385\ (Q_s/Q_w)^{0.412}$) topset slope values, the size of the fluvial envelope (or buffer) acting over the autogenic storage and release events can be estimated. The slope range of the fluvial envelope, $\Delta S = S_{t_\max} - S_{t_\min}$, increases with the Q_s/Q_w ratio. For example, MwLs has a Q_s/Q_w ratio of 0.03 and MwHs has a Q_s/Q_w ratio of 0.123 (Table 1), and this difference is expected to increase in the slope range and thus in size of the fluvial envelope. Only considering the sediment discharge control without the envelope-size modification, it might be expected that the autogenic timescale would linearly decreases with an increase in Q_s; however, when the fluvial envelope enlarges due to an increase in the Q_s/Q_w ratio, more time is necessary to fill a bigger envelope. In other words, comparing MwHs and MwLs, it should be expected that a four times longer autogenic timescale would result from a fourfold decrease in the sediment supply rate; however, MwLs only shows an approximately 1.5 times longer autogenic timescale (Table 1). As shown in Figure 9a, the concave-up pattern in these three lines (i.e., the decreasing rate of the decrease in timescale with an increase in Q_s) reflects the envelope enlargement with Q_s.

[20] Considering Table 1, the normalized autogenic timescales actually show the opposite trend that was calculated from the data, i.e., the timescale increases (frequency decreases) with increasing sediment discharge. Recall that the equilibrium timescale T_{DC} from equation (6b) was used to normalize the experimental data. T_{DC} is a function of sediment discharge, average channel depth and average slope over a measured basin width. Therefore, using this normalization, changes in the fluvio-deltaic system due to differences in the external conditions, e.g., different sediment supplies in different experiments, are minimized. The increase in the autogenic timescale shows the relative increase in the size of the fluvial envelope with increasing sediment discharge. In other words, the longer normalized timescale in the high sediment supply runs reflects a relatively larger space to fill in the fluvial system with a given normalized sediment supply (Figure 10b). The trend in Figure 10b suggests that T_A likely becomes close to T_{DC} and thus $T_A/T_{DC} = 1$ for systems with low Q_s/Q_w.

[21] In summary, size of the fluvial envelope and the available sediment supply to fill this space determine the timescale. Assuming a constant envelope size, increasing the amount of sediment supply would intuitively cause a proportionally shorter autogenic timescale (i.e., primary sediment control). However, as the sediment supply is doubled, the frequency of release events is not doubled (i.e., secondary sediment control) due to the modified envelope size associated with different sediment supply conditions.

5.2. Role of Water Discharge on Autogenic Timescales

[22] Varying water discharge and holding sediment discharge constant affects the autogenic event timescale as well. In general, as water discharge increases, the autogenic timescale increases (frequency decreases). In Figure 9b, sediment discharge is not changing for each set of three experiments, so the changes in Q_w, are mainly responsible for the increase in timescale. An important control in this aspect is the sediment transport capacity of the system, which decreases with a decrease in water discharge [*Bryant et al.*, 1995; *Whipple et al.*, 1998]. A decrease in the capacity for the system to transport sediments causes smaller channels and thus less sediment to be delivered into the basin but more sediment to fill the fluvial buffer space. This high net deposition on the fluvial surface is a factor in decreasing the autogenic timescale with a decrease in water discharge (Figure 9b). The amount of Q_w also affects the autogenic frequency by affecting the organization of the fluvial system (flow pattern). As Q_w decreases, a more organized, channelized system is less likely to develop during the release stages (Figure 5b). For example, consider the first row in the design matrix (Figure 1), experiments LwLs, MwLs, and HwLs. The water discharge in HwLs was the maximum among these experiments (65 cm^3/s), and the

fluvial system was highly organized during release events (i.e., the channelization was pronounced and the channel was deep and straight in geometry). However, in experiments MwLs and LwLs, a successively decreasing amount of water discharge caused the channels to become much more braided and less stable in nature even during their sediment release stages. A lower water discharge caused a narrower range of the fluvial pattern change between the small multiple channels and only partly channelized flows. This created a smaller fluvial envelope and thus, shortened the time that it takes to switch between release and storage processes. In contrast, a higher water discharge caused a wide range of the fluvial pattern change from fully braided to a few deep channels, which strongly reworks the fluvial surface and creates a larger fluvial envelope. The magnitude of release events also increases with increasing water discharge. Instead of small, short pulses during release events (e.g., LwLs), the release events come in long stable periods of progradation (e.g., HwLs) due to stability in the organizational nature of the fluvial system.

5.3. Role of Sediment Discharge to Water Discharge Ratio

[23] The sediment discharge to water discharge ratio contributes to the roughness of the map-view shoreline geometry (i.e., strong local lobe progradation). A smoother shoreline is mainly caused by the frequent autogenic processes as the Q_s/Q_w ratio increases (Figure 5b). Frequent autogenic storage and release processes allow for sediment dispersal across the perimeters of the shoreline to be more uniform, resulting in smoother shoreline geometries. The roughness is also related the fact that the magnitude of release events with a higher Q_s/Q_w ratio is smaller than the magnitude of release events with a lower Q_s/Q_w ratio for individual autogenic events. While there have been other studies that have shown shoreline roughness can be affected by other factors such as sediment mixtures and cohesiveness [*Martin et al.*, 2009b], it is shown here that autogenic storage and release processes can also affect the shoreline roughness (Figure 5).

[24] The ratio of Q_s/Q_w is negatively correlated with the autogenic timescale (Figure 10a). However, experiments with the same Q_s/Q_w ratio did not result in strictly the same timescale values. For instance, consider experiments HwHs, MwMs, and LwLs, which have the same Q_s/Q_w ratio but different values of Q_s and Q_w. First, this indicates that there is a correlation between Q_s and timescale, but the autogenic timescales associated with the lower ratios show wider variation under the same magnitude changes in Q_s. The interplay between the secondary Q_s effect and the Q_w control on the change in the fluvial envelope operates differently to the systems with various Q_s/Q_w ratios and sets up the internal timescale.

[25] While a range of timescales exists for a given Q_s/Q_w ratio, quantitatively it is still unknown how to predict the interplay between the two controls on the fluvial envelope-size modification, but it can be shown that this range is not constant over all ratios. Figure 10a shows that the autogenic timescale curves, grouped by experiments with constant water discharge values, diverge with lower Q_s/Q_w ratios and converge with higher ratios. At higher Q_s/Q_w ratios, there is less variation in autogenic timescales, while at lower ratios, there is more variation in autogenic timescales. Differential effectiveness of Q_s and Q_w controls on the fluvial evolution under different ratios mainly accounts for this variation. As shown here, sediment discharge primarily affects the rate of filling of the fluvial envelope and secondarily influences the size of the envelope created during autogenic release events, while water discharge affects the overall organization of the fluvial system. These controls interact with each other, resulting in the autogenic frequency for given values of Q_s and Q_w. However, even if both of the Q_s and Q_w values change with the same rate, the effects of each Q_s and Q_w controls on the fluvial autogenic processes change with different rates under a given Q_s/Q_w ratio. For instance, from experiment HwMs to MwLs, the Q_s/Q_w ratio remains the same at 0.03, but there are twofold decreases in both water discharge and sediment supply. The autogenic timescale is 0.592 h for HwMs and 0.714 h for MwLs (Table 1), and thus, about a 1.2 times increase in the autogenic timescale. However, the MwHs and LwMs experiments, both keeping the Q_s/Q_w ratio at 0.123 and the same twofold change in water discharge and sediment supply, do not show (or very slightly show) an increase in the autogenic timescale (0.5 h for both MwHs and LwMs). It would be expected to see the same twofold decrease in the timescale for these two sets of experiments assuming linear variations in the response of the autogenic processes to the discharge controls.

[26] Understanding the differential effectiveness of the Q_s and Q_w controls is challenging due to the interplay between these two controls on modifying the fluvial envelope. An assessment of this complex behavior by predicting the autogenic timescales for the experiments is given here. We took ΔS (= $S_{t_\max} - S_{t_\min}$), L_s an averaged shoreline position at the end of all runs, and B^* a characteristic fraction of the fluvial surface occupied by flow in order to estimate the fluvial envelope size as $V_{env} = [B^* \pi (L_s)^3 \Delta S]/12$. The range of slopes ΔS was taken from the formulation given in Figure 6 and a roughly averaged value L_s = 80 cm was applied to all experiments in the prediction for simplicity. Regarding the flow occupation, no data for the wetted fraction of the fluvial surface was collected, but a relationship between B^* and Q_w was generated by calculating the B^* values that account for the observed autogenic timescales using the given ΔS and L_s (Figure 11a) and by running the regression on all of the B^* values. We used this regression relationship ($B^* = 0.031\ (Q_w)^{0.546}$) to apply B^* to the individual experiments. The autogenic timescale was then predicted by $T_A = V_{env}/Q_s$. The timescale prediction fairly captures the observed data (Figure 11b).

[27] The key understanding for the Q_s and Q_w controls on the size of the fluvial envelope is how does ΔS relate to Q_s/Q_w and how does B^* change in response to a change in Q_w. ΔS and B^* increases with Q_s/Q_w and Q_w, respectively, but the increase rates diminish with higher Q_s/Q_w and Q_w. Both ΔS and B^* are positively related to the size of the fluvial envelope, but as Q_w increases, Q_s/Q_w decreases, and thus there is a complex feedback between changes in depth and width of the fluvial buffer to vary the total size of the envelope. In general, at a higher water discharge, a highly organized, stable fluvial system with strong channelization reworks a broader fluvial surface. However, the rate of increase in surface area reworked by the flow with increase in Q_w exponentially decreases and only a minimum impact on

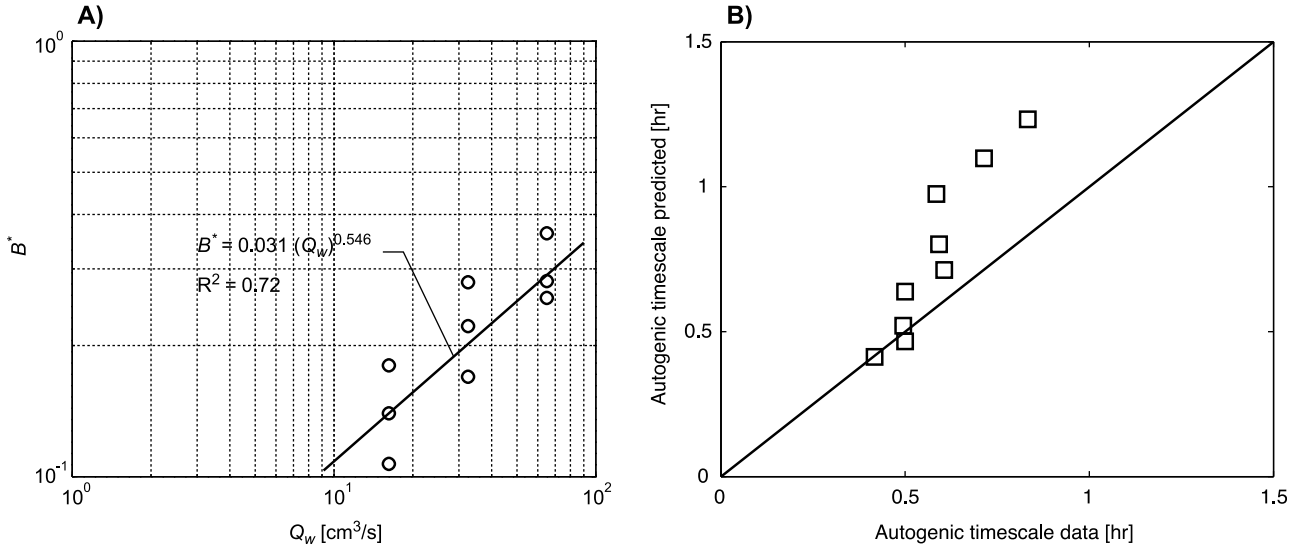

Figure 11. (a) Plot showing a relationship between a characteristic wet-surface fraction and water discharge and (b) comparisons between the observed and predicted autogenic timescales.

the fluvial buffer size modification due to a change in Q_w would be applied for the high Q_w systems. In this Q_w regime, therefore the autogenic timescale can be linearly interpreted using sediment supply. In contrast, at higher Q_s/Q_w ratios (relatively low Q_w), the secondary effects of sediment supply changes and the effect of water discharge changes are maximized. Small changes of Q_s and Q_w in this regime would cause large differences in the fluvial envelope size. The fluvial system is under an unstable regime and causes a more stochastic behavior of the fluvial organization by freely deforming surficial pattern. In these conditions, the accuracy to predict the autogenic timescale using the primary sediment control (reduction in the autogenic timescale by an increased filling rate) is significantly dampened, while the fluvial modification is more significant.

[28] The timescale divergence is highlighted further when considering experiments from previous studies [*Kim and Jerolmack*, 2008]. Experiments from the Experimental Earthscape (XES) facility, XES 02 and XES 05, are reported by *Kim and Jerolmack* [2008], *Kim et al.* [2006a], and *Kim and Paola* [2007]. The XES 02 experiment used 5 times larger sediment and water discharges than XES 05, but the Q_s/Q_w ratios for both experiments were consistently kept at ~0.01, which is lower than the lowest ratio considered in this study. In XES 02, a 3–5 times shorter autogenic timescale was observed compared to that in XES 05 (i.e., approximately T_A = 2–3 h for XES 02 and T_A = 8–10 h for XES 05) [*Kim and Jerolmack*, 2008]. Considering the primary sediment discharge control, a fivefold increase in the sediment discharge could induce a fivefold decrease in the autogenic timescale because of the higher sediment supply available to fill the fluvial envelope. The value that was observed from the two XES 02 and 05 experiments is close to this prediction. These two experiments show that even slightly lower Q_s/Q_w ratios have a much wider range of autogenic timescales, highlighting the divergence occurring at lower ratios due to the more organized system that reflects different sediment supply rates.

5.4. Implications for Stratigraphy and Field Cases

[29] Autogenic storage and release processes can be recognized in fluvial systems in the form of terrace formation. While changes in environmental conditions are important, autogenic incision is another mechanism for generating multiple terraces in fluvial environments [*Muto and Steel*, 2004]. In the experiments presented here, terrace development was observed, but temporary in nature due to stationary base-level conditions. *Erkens et al.* [2009] explore terrace levels in the northern Upper Rhine Graben for the past 20 ky. They show five terrace levels that are different in terms of their elevations, morphologies, and sediment characteristics and argue for allogenic and autogenic controls on the formation of the terrace levels. While older terrace levels formed due to incision attributed to climatic variation and a distinct change from a braided to meandering system, autogenic controls could offer an alternative interpretation for the younger Holocene terraces. *Erkens et al.* [2009] also suspected that autogenic incision would affect Holocene terraces in the Upper Rhine Graben because the Graben was subsiding such that deposition was more dominant than erosion, and environmental conditions during the Holocene were rather consistent. For the most part, allogenic changes in climate were interpreted to be the cause for terrace development; however, autogenic factors should also be considered for an alternative explanation.

[30] The understanding of autogenic storage and release processes is also important for stratigraphic interpretation in terms of source to sink sediment deposition and development of erosional boundaries. Fluvial-dominated deltas at the shelf edge are efficient for delivering high volumes of sediment into the deep-water slope and basin floor environments [*Carvajal and Steel*, 2009; *Edwards*, 1981; *Porębski and Steel*, 2003; *Berg*, 1982]. It is generally accepted that alterations in external forcing are the major control for variations in sediment delivery from deltas into deep water as basin floor fans and sediment supply for turbidites [*Carvajal and Steel*, 2009; *Kolla and Perlmutter*,

1993; *Johannessen and Steel*, 2005]. Consider two basins with a sandy deltaic system at or near the shelf edge feeding sediment into the basin. One has a Q_s/Q_w ratio comparable to HwLs, and the other is comparable to LwLs. The storage and release process occurring on these two deltas would be quite different, and this would impact the deposits on the slope or in the basin. The HwLs delta would have longer duration and larger magnitude autogenic sediment delivery possibly causing turbidity flows and turbidite deposits in thick unified successions separated by periods of storage, or non-deposition on the slope/basin floor. In the case of the LwLs delta, sediment delivery would be short and low magnitude, but it would happen more frequently. This might cause autogenic sediment deposition to result in thin sandy layers from the delta overlain by thin layers of fine-grained sediments that settle out from suspension. This sort of interpretation can also be applied to the Miocene Marnoso-arenacea Formation, northern Apennines [*Lucchi and Valmori*, 1980]. *Lucchi and Valmori* [1980] analyzed basin plain turbidite deposits, and 80–90% of the facies in the 200 m section change in thickness above and below the Contessa marker. An interpretation for the turbidite deposits that are thinner and more numerous in the post-Contessa section as compared to the deposits that are thicker and less numerous in the pre-Contessa section could be attributed to a relative decrease in the source water discharge similar to the change in source discharge conditions from HwLs to LwLs. It is important to acknowledge that changes in stacking pattern at the depositional sink can be a signature of changes in the autogenic storage and release mechanisms of the fluvio-deltaic source system.

6. Conclusions

[31] The present set of experiments with a range of Q_s and Q_w provides a better understanding about how changes in sediment supply and water discharge affect autogenic timescales and also how autogenic storage and release events can be significant for field examples. The experimental results have shown that the relationships between Q_s, Q_w, and Q_s/Q_w are quite complex in relation to the timescale of autogenic storage and release events, but there are important correlations as summarized below.

[32] 1. The evolution of a radially growing, three-dimensional deltaic shoreline can be analytically modeled as function of the cube root of time ($t^{1/3}$), capturing the pattern of the shoreline and shelf edge trajectory.

[33] 2. Increasing the sediment supply in a deltaic system will primarily decrease the autogenic timescale. However, the increase in sediment supply does not proportionally reduce the autogenic timescale because the increase in sediment supply yields the secondary effect on the morphology of the fluvial system by developing a relatively larger fluvial buffer to be filled during times of sediment storage.

[34] 3. Increasing the water discharge in a deltaic system will lengthen the autogenic timescale by shaping the larger fluvial system while it deforms to a more highly organized channel network. This highly organized pattern tends to take a longer time to develop and increases the time necessary for storage and release processes.

[35] 4. The timescale of autogenic storage and release events is negatively correlated with the Q_s/Q_w ratio between 0.015 and 0.246 in the nine experiments presented here. However, complicated interplay between the secondary effects by the Q_s/Q_w ratio on ΔS and the individual value of Q_w on B^* yields a range of autogenic timescales for a given ratio. This indicates the differential effectiveness of the Q_s and Q_w controls on the fluvial evolution under different Q_s/Q_w ratios. The secondary effects of sediment supply diminish at lower ratios while the effects of water discharge enhance at lower ratios, and vice versa. The range of autogenic timescales tends to increase with a smaller ratio and narrows with a larger ratio.

[36] 5. Experiments conducted under changes of boundary conditions in terms of the rate and amplitude of sea-level rise/fall and also basin configuration are important to gain first order understandings in how relative base level affects these internally generated processes, and should formulate interesting future research topics.

Notation

Q_s Sediment discharge, cm^3s^{-1}.
Q_w Water discharge, cm^3s^{-1}.
S_t Topset slope, dimensionless.
S_f Foreset slope, dimensionless.
s Downstream shoreline position, cm.
u Downstream delta toe position, cm.
Z Absolute base level, cm.
H Upstream topset height, cm
t Time, s.
α Constant.
β Constant.
p Constant.
L Characteristic basin length, cm.
h Channel depth, cm.
T_{DC} Equilibrium timescale, s.
B^* Fraction of the fluvial surface occupied by flow.
L_s Averaged shoreline position at the end of experiment, cm.
$S_{t_\min}$ Minimum topset slope.
$S_{t_\max}$ Maximum topset slope.

[37] **Acknowledgments.** This study was supported by a Jackson School of Geosciences at the University of Texas at Austin research grant and a postdoctoral fellowship in Japan Society for the Promotion of Science (JSPS) to W.K and the William R. Muehlberger Scholarship to E.P. We would like to thank Meredith Reitz, Douglas Jerolmack, Paul Heller, Maarten Kleinhans, Simon Mudd, and Alexander Densmore for their constructive comments on the paper.

References

Ashmore, P. (1991), Channel morphology and bed load pulses in braided, gravel-bed streams, *Geogr. Ann., Ser. A*, *73*(1), 37–52, doi:10.2307/521212.

Ashworth, P. J., J. L. Best, and M. Jones (2004), Relationship between sediment supply and avulsion frequency in braided rivers, *Geology*, *32*(1), 21–24, doi:10.1130/G19919.1.

Berg, O. R. (1982), Seismic detection and evaluation of delta and turbidite sequences: Their application to exploration for the subtle trap, *AAPG Bull.*, *66*(9), 1271–1288.

Bryant, M., P. Falk, and C. Paola (1995), Experimental study of avulsion frequency and rate of deposition, *Geology*, *23*(4), 365–368, doi:10.1130/0091-7613(1995)023<0365:ESOAFA>2.3.CO;2.

Carvajal, C. R., and R. J. Steel (2006), Thick turbidite successions from supply-dominated shelves during sea-level highstand, *Geology*, *34*(8), 665–668, doi:10.1130/G22505.1.

Carvajal, C., and R. Steel (2009), Shelf-edge architecture and bypass of sand to deep water: Influence of shelf-edge processes, sea level, and sediment supply, *J. Sediment. Res.*, *79*, 652–672, doi:10.2110/jsr.2009.074.

Cazanacli, D., C. Paola, and G. Parker (2002), Experimental steep, braided flow: Application to flooding risk on fans, *J. Hydraul. Eng.*, *128*, 322–330, doi:10.1061/(ASCE)0733-9429(2002)128:3(322).

Edwards, M. B. (1981), Upper Wilcox Rosita delta system of south Texas; growth-faulted shelf-edge deltas, *AAPG Bull.*, *65*, 54–73.

Erkens, G., R. Dambeck, K. P. Volleberg, M. T. I. J. Bouman, J. A. A. Bos, K. M. Cohen, J. Wallinga, and W. Z. Hoek (2009), Fluvial terrace formation in the northern Upper Rhine Graben during the last 20,000 years as a result of allogenic controls and autogenic evolution, *Geomorphology*, *103*, 476–495, doi:10.1016/j.geomorph.2008.07.021.

Galloway, W. E. (1989a), Genetic stratigraphic sequences in basin analysis, part I: Architecture and genesis of flooding-surface bounded depositional units, *AAPG Bull.*, *73*, 125–142.

Galloway, W. E. (1989b), Genetic stratigraphic sequences in basin analysis, part II: Application to northwest Gulf of Mexico Cenozoic basin, *AAPG Bull.*, *73*, 143–154.

Gerber, T. P., L. F. Pratson, M. A. Wolinsky, R. Steel, J. Mohr, J. B. Swenson, and C. Paola (2008), Clinoform progradation by turbidity currents: Modeling and experiments, *J. Sediment. Res.*, *78*, 220–238, doi:10.2110/jsr.2008.023.

Helland-Hansen, W., and J. G. Gjelberg (1994), Conceptual basis and variability in sequence stratigraphy: A different perspective, *Sediment. Geol.*, *92*, 31–52, doi:10.1016/0037-0738(94)90053-1.

Helland-Hansen, W., and O. J. Martinsen (1996), Shoreline trajectories and sequences; description of variable depositional-dip scenarios, *J. Sediment. Res.*, *66*, 670–688, doi:10.1306/D42683DD-2B26-11D7-8648000102C1865D.

Heller, P. L., B. A. Burns, and M. Marzo (1993), Stratigraphic solution sets for determining the roles of sediment supply, subsidence, and sea level on transgressions and regressions, *Geology*, *21*, 747–750, doi:10.1130/0091-7613(1993)021<0747:SSSFDT>2.3.CO;2.

Heller, P. L., C. Paola, I.-G. Hwang, B. John, and R. J. Steel (2001), Geomorphology and sequence stratigraphy due to slow and rapid base-level changes in an experimental subsiding basin (XES 96-1), *AAPG Bull.*, *85*, 817–838, doi:10.1306/8626CA0F-173B-11D7-8645000102C1865D.

Hickson, T. A., B. A. Sheets, C. Paola, and M. Kelberer (2005), Experimental test of tectonic controls on three-dimensional alluvial facies architecture, *J. Sediment. Res.*, *75*, 710–722, doi:10.2110/jsr.2005.057.

Hogg, S. E. (1982), Sheetfloods, sheetwash, sheetflow, or …?, *Earth Sci. Rev.*, *18*, 59–76, doi:10.1016/0012-8252(82)90003-4.

Holbrook, J., R. W. Scott, and F. E. Oboh-Ikuenobe (2006), Base-level buffers and buttresses: A model for upstream versus downstream control on fluvial geometry and architecture within sequences, *J. Sediment. Res.*, *76*, 162–174, doi:10.2110/jsr.2005.10.

Jerolmack, D. J., and D. Mohrig (2005), Frozen dynamics of migrating bedforms, *Geology*, *33*(1), 57–60, doi:10.1130/G20897.1.

Johannessen, E. P., and R. J. Steel (2005), Shelf-margin clinoforms and prediction of deepwater sands, *Basin Res.*, *17*, 521–550, doi:10.1111/j.1365-2117.2005.00278.x.

Kim, W., and D. J. Jerolmack (2008), The pulse of calm fan deltas, *J. Geol.*, *116*, 315–330, doi:10.1086/588830.

Kim, W., and T. Muto (2007), Autogenic response of alluvial-bedrock transition to base-level variation: Experiment and theory, *J. Geophys. Res.*, *112*, F03S14, doi:10.1029/2006JF000561.

Kim, W., and C. Paola (2007), Long-period cyclic sedimentation with constant tectonic forcing in an experimental relay ramp, *Geology*, *35*(4), 331–334, doi:10.1130/G23194A.1.

Kim, W., C. Paola, J. B. Swenson, and V. R. Voller (2006a), Shoreline response to autogenic processes of sediment storage and release in the fluvial system, *J. Geophys. Res.*, *111*, F04013, doi:10.1029/2006JF000470.

Kim, W., C. Paola, V. R. Voller, and J. B. Swenson (2006b), Experimental measurement of the relative importance of controls on shoreline migration, *J. Sediment. Res.*, *76*(2), 270–283, doi:10.2110/jsr.2006.019.

Kim, W., B. A. Sheets, and C. Paola (2010), Steering of experimental channels by lateral basin tilting, *Basin Res.*, *22*, 286–301, doi:10.1111/j.1365-2117.2009.00419.x.

Kleinhans, M. G. (2005), Autogenic cyclicity of foreset sorting in experimental Gilbert-type deltas, *Sediment. Geol.*, *181*, 215–224, doi:10.1016/j.sedgeo.2005.09.001.

Kleinhans, M. G., H. E. van de Kasteele, and E. Hauber (2010a), Palaeoflow reconstruction from fan delta morphology on Mars, *Earth Planet. Sci. Lett.*, *294*(3–4), 378–392, doi:10.1016/j.epsl.2009.11.025.

Kleinhans, M. G., H. J. T. Weerts, and K. M. Cohen (2010b), Avulsion in action: Reconstruction and modelling sedimentation pace and upstream flood water levels following a Medieval tidal-river diversion catastrophe (Biesbosch, the Netherlands, 1421–1750 AD), *Geomorphology*, *118*, 65–79, doi:10.1016/j.geomorph.2009.12.009.

Kolla, V., and M. A. Perlmutter (1993), Timing of turbidite sedimentation on the Mississippi Fan, *AAPG Bull.*, *77*(7), 1129–1141.

Kostic, S., G. Parker, and J. G. Marr (2002), Role of turbidity currents in setting the foreset slope of clinoforms prograding into standing fresh water, *J. Sediment. Res.*, *72*(3), 353–362, doi:10.1306/081501720353.

Lorenzo-Trueba, J., V. R. Voller, T. Muto, W. Kim, C. Paola, and J. B. Swenson (2009), A similarity solution for a dual moving boundary problem associated with a coastal-plain depositional system, *J. Fluid Mech.*, *628*, 427–443, doi:10.1017/S0022112009006715.

Lucchi, F. R., and E. Valmori (1980), Basin-wide turbidites in a Miocene, over-supplied deep-sea plain: A geometrical analysis, *Sedimentology*, *27*, 241–270, doi:10.1111/j.1365-3091.1980.tb01177.x.

Martin, J., C. Paola, V. Abreu, J. Neal, and B. Sheets (2009a), Sequence stratigraphy of experimental strata under known conditions of differential subsidence and variable base level, *AAPG Bull.*, *93*, 503–533, doi:10.1306/12110808057.

Martin, J., B. Sheets, C. Paola, and D. Hoyal (2009b), Influence of steady base-level rise on channel mobility, shoreline migration, and scaling properties of a cohesive experimental delta, *J. Geophys. Res.*, *114*, F03017, doi:10.1029/2008JF001142.

Mohrig, D., P. L. Heller, C. Paola, and W. J. Lyons (2000), Interpreting avulsion process from ancient alluvial sequences: Guadalope-Matarranya system (northern Spain) and Wasatch Formation (western Colorado), *Geol. Soc. Am. Bull.*, *112*(12), 1787–1803, doi:10.1130/0016-7606(2000)112<1787:IAPFAA>2.0.CO;2.

Muto, T. (2001), Shoreline autoretreat substantiated in flume experiments, *J. Sediment. Res.*, *71*(2), 246–254, doi:10.1306/091400710246.

Muto, T., and H. Okada (1991), A comment on modelling the paleogeography of confined and unconfined marine Gilbert-type deltas, *Cuad. Geol. Iber.*, *15*, 139–162.

Muto, T., and R. J. Steel (2001), Autostepping during the transgressive growth of deltas: Results from flume experiments, *Geology*, *29*(9), 771–774, doi:10.1130/0091-7613(2001)029<0771:ADTTGO>2.0.CO;2.

Muto, T., and R. J. Steel (2004), Autogenic response of fluvial deltas to steady sea-level fall: Implications from flume-tank experiments, *Geology*, *32*(5), 401–404, doi:10.1130/G20269.1.

Muto, T., and J. B. Swenson (2006), Autogenic attainment of large-scale alluvial grade with steady sea-level fall: An analog tank-flume experiment, *Geology*, *34*(3), 161–164, doi:10.1130/G21923.1.

Muto, T., R. J. Steel, and J. B. Swenson (2007), Autostratigraphy: A framework norm for genetic stratigraphy, *J. Sediment. Res.*, *77*(1), 2–12, doi:10.2110/jsr.2007.005.

Paola, C. (2000), Quantitative models of sedimentary basin filling, *Sedimentology*, *47*, suppl. 1, 121–178, doi:10.1046/j.1365-3091.2000.00006.x.

Paola, C., et al. (2001), Experimental stratigraphy, *GSA Today*, *11*, 4–9, doi:10.1130/1052-5173(2001)011<0004:ES>2.0.CO;2.

Paola, C., K. Straub, D. Mohrig, and L. Reinhardt (2009), The "unreasonable effectiveness" of stratigraphic and geomorphic experiments, *Earth Sci. Rev.*, *97*, 1–43, doi:10.1016/j.earscirev.2009.05.003.

Parker, G., C. Paola, K. X. Whipple, and D. Mohrig (1998), Alluvial fans formed by channelized fluvial and sheet flow. Part I: Theory, *J. Hydraul. Eng.*, *124*, 985–995, doi:10.1061/(ASCE)0733-9429(1998)124:10(985).

Petter, A. L., and T. Muto (2008), Sustained alluvial aggradation and autogenic detachment of the alluvial river from the shoreline in response to steady fall of relative sea level, *J. Sediment. Res.*, *78*, 98–111, doi:10.2110/jsr.2008.012.

Porębski, S. J., and R. J. Steel (2003), Shelf-margin deltas: Their stratigraphic significance and relation to deepwater sands, *Earth Sci. Rev.*, *62*, 283–326, doi:10.1016/S0012-8252(02)00161-7.

Posamentier, H. W., and P. R. Vail (1988), Eustatic controls on clastic deposition. Part II—Sequence and systems track models, in *Sea-Level Changes*, *Spec. Publ. Soc. Econ. Paleontol. Mineral.*, vol. 42, edited by C. K. Wilgus et al., pp. 125–154, Soc. of Econ. Paleontol. and Mineral., Tulsa, Okla.

Posamentier, H. W., M. T. Jervey, and P. R. Vail (1988), Eustatic controls on clastic deposition. Part I—Conceptual framework, in *Sea-Level Changes*, *Spec. Publ. Soc. Econ. Paleontol. Mineral.*, vol. 42, edited by C. K. Wilgus et al., pp. 109–124, Soc. of Econ. Paleontol. and Mineral., Tulsa, Okla.

Postma, G., M. G. Kleinhans, P. T. Meijer, and J. T. Eggenhuisen (2008), Sediment transport in analogue flume models compared with real-world sedimentary systems: A new look at scaling evolution of sedimentary systems in a flume, *Sedimentology*, *55*, 1541–1557, doi:10.1111/j.1365-3091.2008.00956.x.

Reitz, M. D., D. J. Jerolmack, and J. B. Swenson (2010), Flooding and flow path selection on alluvial fans and deltas, *Geophys. Res. Lett.*, *37*, L06401, doi:10.1029/2009GL041985.

Sheets, B. A., T. A. Hickson, and C. Paola (2002), Assembling the stratigraphic record: Depositional patterns and time-scales in an experimental alluvial basin, *Basin Res.*, *14*, 287–301, doi:10.1046/j.1365-2117.2002.00185.x.

Swenson, J. B., V. R. Voller, C. Paola, G. Parker, and J. G. Marr (2000), Fluvio-deltaic sedimentation: A generalized Stefan problem, *Eur. J. Appl. Math.*, *11*, 433–452, doi:10.1017/S0956792500004198.

Vail, P. R., R. M. Mitchum Jr., and S. Thompson III (1977), Seismic stratigraphy and global changes of sea level, part 3: Relative changes of sea level from coastal onlap, in *Seismic Stratigraphy: Applications to Hydrocarbon Exploration*, *Mem. Am. Assoc. Pet. Geol.*, vol. 26, edited by C. E. Payton, pp. 63–81, Am. Assoc. of Pet. Geol., Tulsa, Okla.

Van Dijk, M., G. Postma, and M. G. Kleinhans (2009), Autocyclic behaviour of fan deltas: An analogue experimental study, *Sedimentology*, *56*, 1569–1589, doi:10.1111/j.1365-3091.2008.01047.x.

Van Wagoner, J. C., H. W. Posamentier, R. M. Mitchum, P. R. Vail, J. F. Sarg, T. S. Loutit, and J. Hardenbol (1988), An overview of the fundamentals of sequence stratigraphy and key definitions, in *Sea-Level Changes*, *Spec. Publ. Soc. Econ. Paleontol. Mineral.*, vol. 42, edited by C. K. Wilgus et al., pp. 39–45, Soc. of Econ. Paleontol. and Mineral., Tulsa, Okla.

Watts, A. B. (1982), Tectonic subsidence, flexure and global changes of sea level, *Nature*, *297*, 469–474, doi:10.1038/297469a0.

Whipple, K. X., G. Parker, C. Paola, and D. Mohrig (1998), Channel dynamics, sediment transport, and the slope of alluvial fans: Experimental study, *J. Geol.*, *106*, 677–694, doi:10.1086/516053.

W. Kim and E. J. Powell, Department of Geological Sciences, Jackson School of Geosciences, University of Texas at Austin, 1 University Sta. C9000, Austin, TX 78712, USA. (ejpowell@utexas.edu)

T. Muto, Graduate School of Fisheries Science and Environmental Studies, Nagasaki University, 1-14 Bunkyomachi, Nagasaki 852-8521, Japan.